Synthesis, Characterization, and Growth Rates of Aluminum- and Ge,Al-Substituted Silicalite-1 Materials Grown from Clear Solutions

Chil-Hung Cheng,[†] Gopalakrishnan Juttu,[§] Scott F. Mitchell,[§] and Daniel F. Shantz*,[†]

Department of Chemical Engineering, Texas A&M University, College Station Texas 77843-3122, SABIC Technology Center, SABIC Americas, Inc., Sugarland, Texas 77478

Received: June 20, 2006; In Final Form: September 3, 2006

The synthesis, characterization, and growth rates of aluminum- and germanium,aluminum-substituted silicalite-1 (Al-silicalite-1, Ge,Al-silicalite-1) materials grown from clear solutions are reported. In the case of aluminum substitution, the crystallinity of the materials as determined by powder X-ray diffraction (PXRD) decreases with increasing aluminum content, as does the micropore volume determined by nitrogen adsorption and the growth rate determined by in situ small-angle X-ray scattering (SAXS). The final materials possess slightly lower Si/Al ratios than the initial synthesis mixtures based on X-ray fluorescence analysis. In the case of simultaneous incorporation of germanium and aluminum, the final materials have a slightly lower Si/Al ratio than the synthesis mixture but a much higher Si/Ge ratio, indicating the aluminum is more readily incorporated in the zeolite as compared to germanium. This result is consistent with studies of individual heteroatom substitution behavior. Germanium incorporation in the final material increases at higher heteroatom contents (Si/(Ge+Al) = 50 and 25). The promoting effect of germanium on the growth rate of silicalite-1 dominates at low heteroatom content (Si/(Ge+Al) = 100), leading to enhanced zeolite growth rates as compared to pure silicalite-1. This promoting effect is insensitive to the Ge/Al ratio at a Si/(Ge+Al) = 100. The influence of aluminum on the growth rate, as well as the crystallinity of final materials, becomes observable when the heteroatom content is increased (Si/(Ge+Al) = 50 and 25). This is the first study we are aware of that reports the synthesis of Ge,Al-substituted silicalite-1 phases formed in hydroxide media or from clear solutions and has implications for the synthesis of nanoparticulate zeolitic materials for catalysis.

Introduction

Given that the catalytic properties of zeolites are often dictated by the presence, number density, and local state of heteroatoms in the zeolite framework, there is clear interest for understanding how the presence of heteroatoms impact zeolite nucleation and growth.[1,2] Zones and co-workers have reported numerous studies of how heteroatom inclusion affects phase selectivity;[3−7] however, investigations of how the heteroatom content influences growth rates and the (in)ability to form different zeolite phases are relatively sparse.

We have recently published work that describes how the inclusion of germanium in silicalite-1 clear solution syntheses impacts the growth of the zeolite phase.[8] That work shows that germanium, while being incompletely incorporated in the framework, enhances the rate of zeolite formation and growth. In this report we expand the scope of that work by investigating how aluminum and mixed germanium/aluminum incorporation affects zeolite growth rates in the so-called clear solution synthesis of silicalite-1. To the best of our knowledge there are no reports in the literature on the growth of Al-silicalite-1 from clear solutions comparable to the pure silica solutions that have been intensely studied.[9−21] That motivated the study of the aluminum-containing solutions. The mixed heteroatom inclusion study was motivated by work from Maschmeyer's lab showing Ge,Al-MFI materials have unusual catalytic properties.[22−24] As such the materials described here are catalytically relevant, and understanding growth rates in the presence of multiple heteroatoms provides new insights for designing zeolite nanocrystals for catalysis.

Experimental Section

Zeolite Syntheses. Aluminum-silicalite-1 (Al-silicalite-1) was synthesized from mixtures of composition *x* TEOS:*z* Al-$(OC_2H_5)_3$:0.36 TPAOH:20 H_2O with Si/Al ratio = 200, 100, 50, and 25 while keeping $x + z = 1$. Aluminum triethoxide ($Al(OC_2H_5)_3$, Aldrich, >97%) was used as the aluminum source. Germanium,aluminum-silicalite-1 (Ge,Al-silicalite-1) was synthesized from mixtures of composition *x* TEOS:*y* GeO_2:*z* Al-$(OC_2H_5)_3$:0.36 TPAOH:20 H_2O with Si/(Al+Ge) ratio = 100, 75, 50, and 25 while keeping $x + y + z = 1$. Germanium dioxide (GeO_2, Aldrich, 99.999%) was used as the germanium source, and aluminum triethoxide ($Al(OC_2H_5)_3$, Aldrich, >97%) was used as the aluminum source. For each Si/(Al+Ge) ratio the Ge/Al ratio was varied from 1 to 4. The synthesis mixtures in all cases were placed in screw-cap Teflon containers and heated at 368 K for 7 days. The solids were collected by centrifugation, washed with deionized water, dried, and characterized by powder XRD. The same solutions were prepared for the in situ SAXS measurements. For clarity, the Si/Al and Si/(Al+Ge) ratios stated in the Discussion Section are those of the synthesis mixture.

Analytical. Powder X-ray diffraction (PXRD) measurements were performed on a Bruker AXS D8 powder diffractometer (Cu Kα radiation) in reflection mode from $2\theta = 4$ to 50° with

* Corresponding author. Phone: (979) 845-3492. Fax: (979) 845-6446. E-mail: shantz@che.tamu.edu.
[†] Texas A&M University.
[§] SABIC Technology Center.

10.1021/jp0638538 CCC: $33.50
Published on Web 10/13/2006

a step size of 0.02° and 5 s per step. The PXRD patterns were indexed using the software program PowderX and were refined using Lapod. Field-emission scanning electron microscopy (FE-SEM) measurements were performed using a Zeiss Leo-1530 microscope operating at 1−10 kV. X-ray fluorescence (XRF) measurements were performed on a Rigaku ZSX100e instrument with a Rh target. The sample was fused with lithium tetraborate before elemental analysis. Nitrogen adsorption experiments were performed on a Micromeritics ASAP 2010 micropore analyzer with a turbo pump capable of obtaining relative pressures of less than 10^{-6}. The samples used in adsorption experiments were calcined to remove the TPAOH by heating from room temperature to 823 K at a rate of 1 K/min and then held at 823 K for 8 h. Samples were degassed at 373 K for 4 h, then at 573 K overnight before performing the measurements. The isotherms were measured over the relative pressure range of 10^{-6} to 0.98. Surface area and pore volumes were determined using the α_s method.[25,26]

The in situ SAXS measurements were performed using the cell and procedures reported previously.[27,28] All the SAXS experiments were performed on a Bruker NanoSTAR system with a Nonius rotating anode (FR591) and a copper target (1.5417 Å), operating at 45 kV and 90 mA. The precursor solution was loaded in a high-temperature cell, and the in situ measurements were performed at 368 K with a measuring period of 1.5 h. Water was used as the reference solvent for background subtraction.

Pair distance distribution functions (PDDFs) were determined from the scattering data using the program GNOM based on the inverse Fourier transform method (IFT).[29−33] For data obtained during the induction period, the particle diameter was determined using the optimized perceptual criteria introduced by Servgun[34] as well as the Guinier approximation.[35] The radius of gyration obtained from the Guinier approximation was calculated assuming a spherical particle geometry. The values obtained from both approaches were almost identical. For scattering patterns measured following the induction period, the particle size distribution was determined to be bimodal. The diameter of the larger particles was determined from the Guinier approximation, and the particle diameter of the smaller particles was determined from the optimized perceptual criteria within the smaller guessing value ranges. The theoretical fitting matched the experimental scattering data in the high q range for this optimized guessing value. However, the low q range data could not be described using just the small particle population. The growth rate during the crystallization period was determined from the particle diameter as a function of the synthesis duration using linear regression.

Results

Aluminum Substitution. Figure 1 shows the PXRD patterns of samples made in the presence of aluminum. The peak widths broaden, and the crystallinity as observable by PXRD decreases with increasing aluminum content. The synthesis duration needed to form Al-silicalite-1 also increases with the aluminum content. Al-Silicalite-1 can be formed within a day at 368 K based on the mixture becoming optically opaque (Si/Al = 200); however, the precursor solution remained transparent for 5 days at Si/Al = 50 before the onset of turbidity. At the highest aluminum content (Si/Al = 25) the mixture remained optically transparent after 28 days of heating, and no solids could be recovered. FTIR (Supporting Information) shows the band assigned to double five-membered ring species at 550 cm^{-1} decreases in intensity with increasing aluminum content. Using IR to assess phase purity of zeolites has resulted in significant contention in the literature,[36] and as such we believe it is qualitative at best. The PXRD results indicate that increasing the aluminum content leads to less crystalline material. Only two well-resolved diffraction peaks can be observed for the sample with a Si/Al = 50. The broad features observed could be due to very small zeolite particles.[37] Two other possibilities are that the yield of zeolite phase is very low or that it is poorly crystalline; nitrogen adsorption (see below) seems consistent with the presence of a poorly crystalline phase. Qualitatively, the results above indicate that the inclusion of aluminum in the synthesis mixture suppresses growth of the zeolite phase. This is quantified below using small-angle X-ray scattering. Table 1 summarizes the XRF results and shows that the materials obtained have a slightly lower Si/Al ratio than the initial synthesis mixture. This result indicates it is possible to incorporate aluminum into the zeolite phase under these conditions. Figure 2 shows the FE-SEM images of the Al-silicalite-1 samples. The particle size decreases with increasing aluminum content and varies from 100 (Si/Al = 200) to approximately 20 (Si/Al = 50) nm. The particle shape becomes less well defined as the aluminum content increases, possibly due to the appearance of amorphous material filling the interparticulate voids.

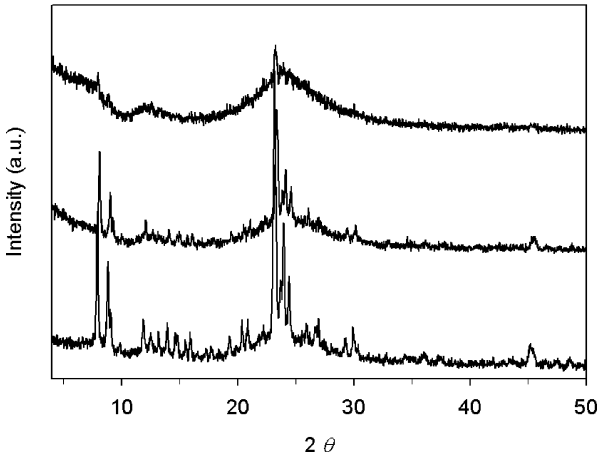

Figure 1. PXRD patterns of Al-silicalite-1 synthesized at 368 K for 7 days. From bottom to top: Si/Al = 200, Si/Al = 100, Si/Al = 50.

TABLE 1: Aluminum Content of Al-silicalite-1 Determined by X-ray Fluorescence Spectroscopy (XRF)

Si/Al, mixture	Si/Al, product
200	142
100	91
50	45

Nitrogen adsorption was also used to characterize the materials obtained. A representative adsorption isotherm is shown in Figure 3; the results for the other samples are tabulated in the Supporting Information. The N_2 adsorption isotherms typically have some degree of micropore filling at low ($p/p_o < 10^{-5}$) pressures, a plateau, then a large amount of nitrogen is adsorbed at high ($p/p_o > 0.8$) pressure. Micropore volumes for samples with Si/Al = 200 and Si/Al = 100 are 0.12 and 0.09 cm^3/g, consistent with a decrease in crystallinity as the Si/Al ratio decreases. The sample with a Si/Al = 50 has no detectable microporosity based on α_s-analysis. This result supports the conclusion that if this sample has any zeolite phase, it is either present in low yield or is poorly crystalline. The appreciable nitrogen adsorbed at high pressures could be due either to

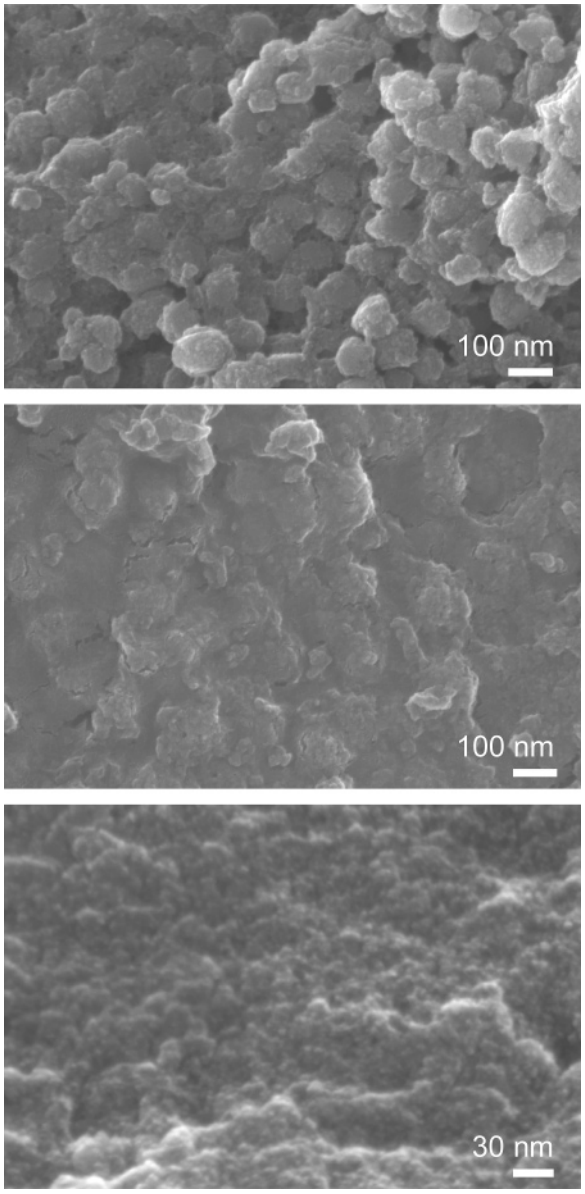

Figure 2. FE-SEM images of Al-silicalite-1 synthesized at 368 K for 7 days. From top to bottom Si/Al = 200, 100, 50.

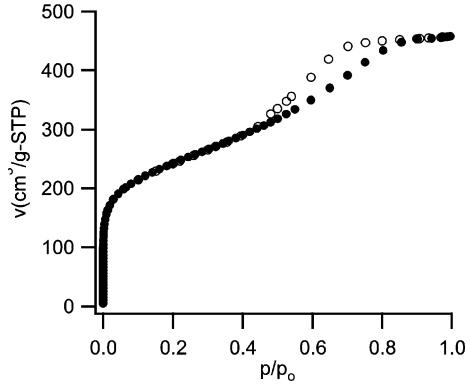

Figure 3. Nitrogen adsorption isotherm for Al-silicalite-1 with a Si/Al = 100. (●) Adsorption loop. (○) Desorption loop.

mesopores or multilayer adsorption in the void spaces between the particles. Given the small particle size we believe it is the latter.

Growth Rate of Al-silicalite-1. The PXRD data indicates that increasing the aluminum content of the synthesis mixture

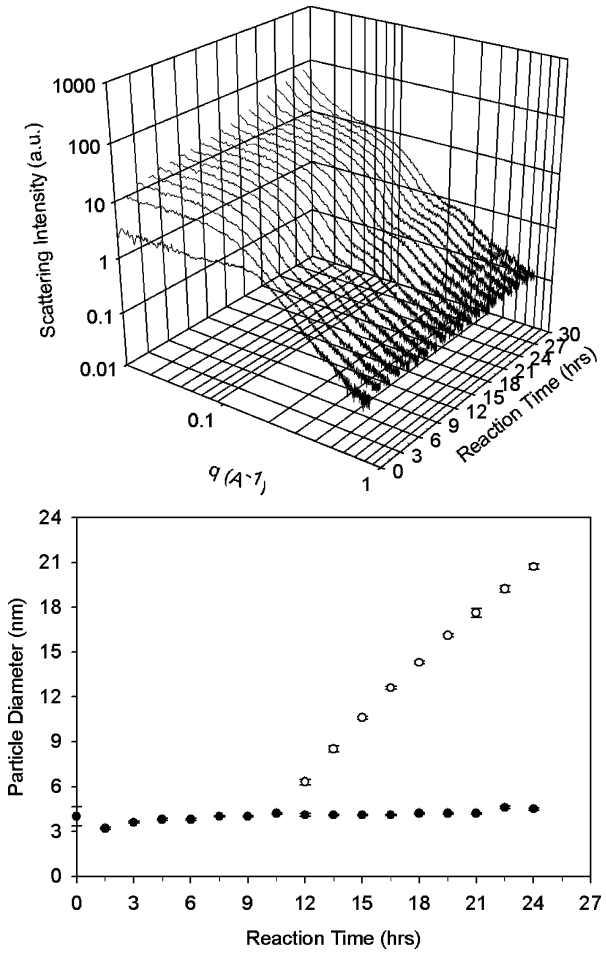

Figure 4. (Top) Time-resolved SAXS scattering patterns of 0.990 TEOS: 0.010 $Al(OC_2H_5)_3$: 0.36 TPAOH: 20 H_2O at 368 K. (Bottom) Plot of particle size versus reaction time.

leads to a decrease in the zeolite growth rate. In situ SAXS measurements were performed to quantify this effect. The time-resolved scattering patterns and the corresponding particle size as a function of the synthesis duration are shown in Figures 4−6. The main growth parameters are summarized in Table 2. Consistent with previous studies[14,17,27,38,39] the particle size distribution of the precursor solution during growth is bimodal for all three compositions studied. The slope of the scattering patterns in the Porod regime is −2.1, indicating the primary particles are nonspherical. The diameter of the primary particles is approximately 4 nm. For a precursor solution with Si/Al = 150, the induction period and the time elapsed until Bragg peaks are first observed in the Porod regime are 6.0−7.5 and 16.5 h respectively, yielding a growth rate of 1.92 ± 0.06 nm/h, close to that of silicalite-1 (1.9 ± 0.1 nm/h).[27] As the aluminum content increases (Si/Al = 120, 100) the induction period increases to 9 and 12 h, respectively, and the particle growth rate decreases to 1.56 ± 0.04 nm/h and 1.22 ± 0.03 nm/h, respectively. Thus, there is a clear correlation between increasing aluminum content in the synthesis mixture and decreasing zeolite growth rates. This result is consistent with Cundy's work, although sodium cations were the hydroxide source in their mixtures.[40] By contrast we have recently published work which shows that the presence of germanium increases zeolite growth rates.[8] To study the effect of aluminum more closely, the initial scattered intensity at zero angle ($I(0)$) is listed in Table 3. Given the presence of particle−particle interactions as manifested as a maximum in the I versus q data, quantitative determination

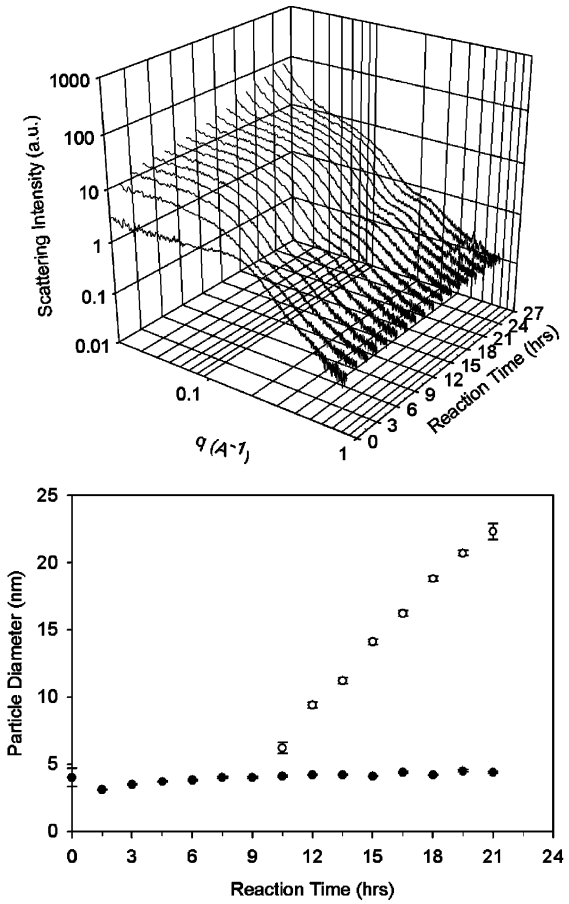

Figure 5. (Top) Time-resolved SAXS scattering patterns of 0.992 TEOS: 0.008 $Al(OC_2H_5)_3$: 0.36 TPAOH: 20 H_2O at 368 K. (Bottom) Plot of particle size versus reaction time.

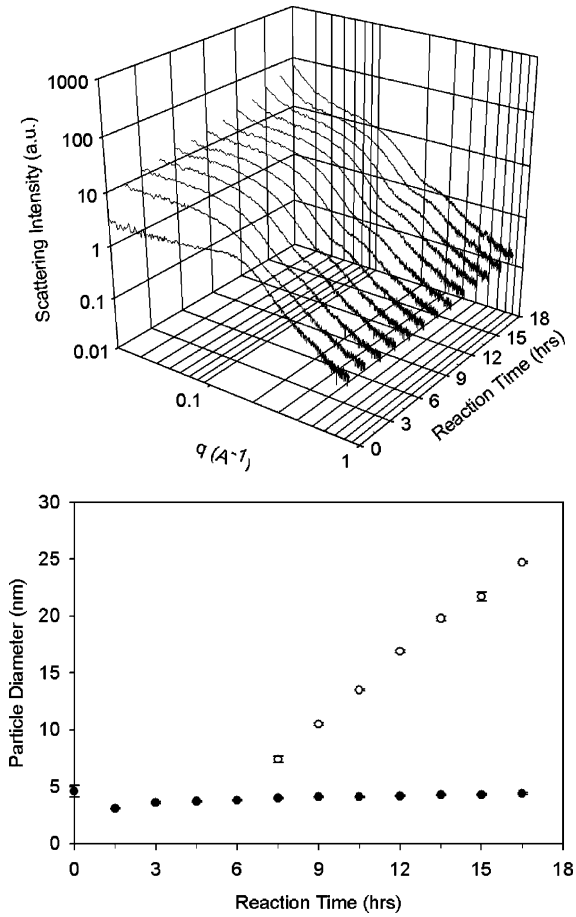

Figure 6. (Top) Time-resolved SAXS scattering patterns of 0.993 TEOS: 0.007 $Al(OC_2H_5)_3$: 0.36 TPAOH: 20 H_2O at 368 K. (Bottom) Plot of particle size versus reaction time.

of the particle number density is not warranted. However, $I(0)$ is a qualitative measure of the number density of particles. The $I(0)$ values (2.2−2.5) indicate the number density of primary particles is essentially invariant to the aluminum content. For comparison the $I(0)$ value for the same mixture *without aluminum* is 6.0.[27] As such, this indicates qualitatively that in the presence of aluminum the number density of particles is lower than in the pure silica case. Thus, the aluminum retards growth and also exerts an influence on the initial number density of particles. This is consistent with the picture that the solution pH and cation solubility are central in determining the particle size/concentration.[41,42] Calculations were also performed to estimate the relative fraction of primary particles and growing particles when the growing particles were approximately 25 nm in diameter. These results are also summarized in Table 3, and the details of the calculations are given in the Supporting Information. From these results, the ratio of primary to growing particles (3.1−2.9) is fairly insensitive to the aluminum content. Comparing this to the pure silicalite-1 material (data taken from ref 27) the ratio for that mixture is 1.78:1 primary/growing particles. On the basis of this analysis it is seen that in the presence of aluminum there is a higher ratio of primary to growing particles as compared to that in the pure silica case. Given the assumptions made (e.g., the small and large particles have the same electron density), it is more appropriate to look at the trends rather than the absolute values.

Mixed Heteroatom Inclusion. Syntheses were also performed to study the mixed substitution of germanium and aluminum. The PXRD patterns of these materials are shown in Figure 7. No distinct difference could be observed from the patterns when Si/(Al+Ge) = 100 and the Ge/Al ratio changes from 4 to 1. The peak widths broaden when the heteroatom content increases, i.e. Si/(Al+Ge) = 50 and Si/(Al+Ge) = 25. At higher aluminum contents the crystallinity decreases with decreasing Ge/Al ratios. In addition, the effect of aluminum on Ge,Al-silicalite-1 particle size only becomes observable at the highest heteroatom content with the Ge/Al ratio of 1 based on SEM images (Supporting Information). The decreasing crystallinity observed by PXRD is confirmed by FTIR and N_2 adsorption results, showing a decrease in intensity of the IR band at 550 cm^{-1} and a significant decrease of the micropore

TABLE 2: Growth Kinetics Summary of Al-silicalite-1 from in Situ SAXS Measurements

Si/Al ratio	duration of induction period (h)	appearance of Bragg diffraction peaks (h)	growth rate (nm/h)
100	10.5−12.0	24.0	1.22 ± 0.03
120	7.5−9.0	21.0	1.56 ± 0.04
150	6.0−7.5	16.5	1.92 ± 0.06

TABLE 3: Initial Scattered Intensity ($I(0)$) and Estimate of the Ratio of Primary Particles to Growing Crystals of Al-silicalite-1 from in Situ SAXS Measurements

Si/Al ratio	$I(0)$ before heating	primary particles/ growing crystals[a] ratio
100	2.5	2.9 (24.0)
120	2.2	3.1 (21.0)
150	2.4	2.9 (16.5)

[a] Heating duration at 368 K (in hours) given in parentheses. In all cases the growing crystals are approximately 25 nm in diameter.

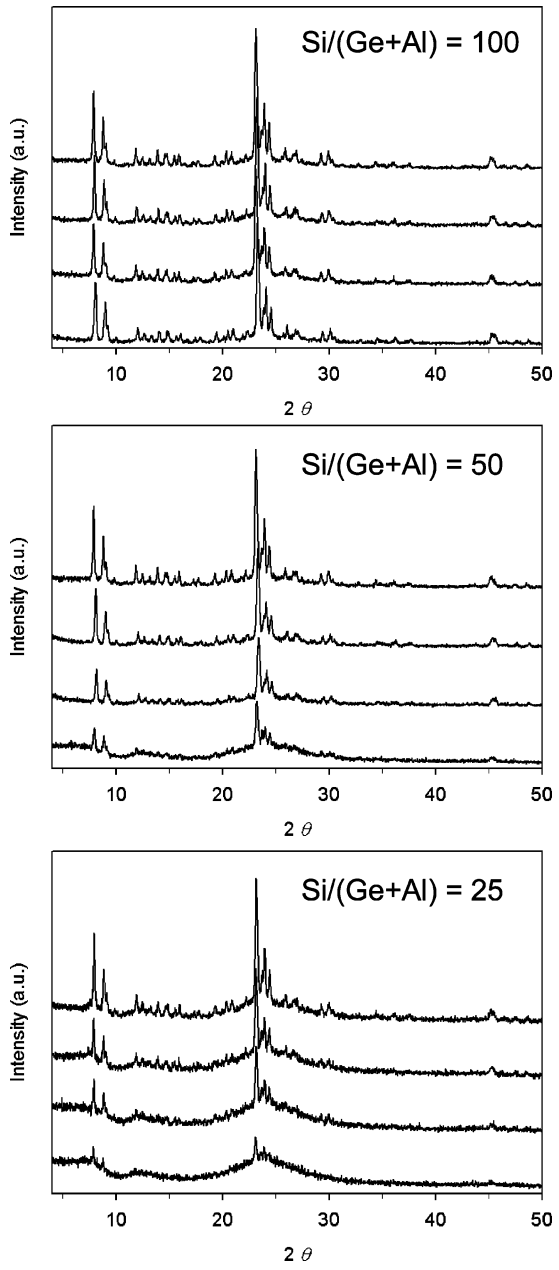

Figure 7. PXRD patterns Ge,Al-silicalite-1 synthesized at 368 K for 7 days with Si/(Ge+Al) ratio = (top to bottom) 100, 50, 25. From bottom to top in each figure Ge/Al = 1, Ge/Al = 2, Ge/Al = 3, Ge/Al = 4.

volume by nitrogen adsorption (Supporting Information). The nitrogen adsorption data shows the micropore volume decreases at a given Si/(Ge+Al) value as the Al content increases, and the micropore volumes trend downward as the total heteroatom content increases. The hypothesis of competing effects between Al and Ge will be further quantified using small-angle X-ray scattering.

The XRF results for the mixed substitution samples are comparable to the case of mixtures with single heteroatom substitution except at the highest substitution levels (Figure 8, tabulated in Supporting Information). The aluminum incorporation appears comparable to the results above when only aluminum substitution was considered. Perhaps more interesting is the incorporation of germanium in the presence of aluminum. At the lowest heteroatom content (Si/(Ge+Al) = 100) the germanium incorporation is fairly low, similar to the syntheses with only germanium.[8] However, as the heteroatom content is

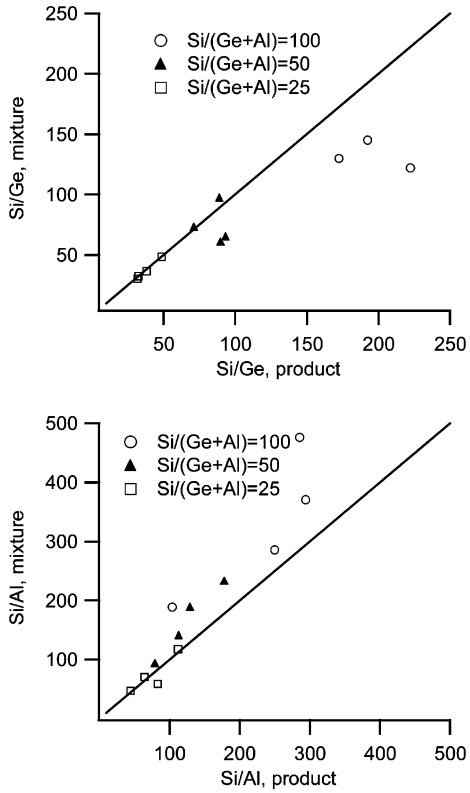

Figure 8. Plots of the XRF data (top, germanium; bottom, aluminum) for silicalite-1 syntheses containing germanium and aluminum.

increased, the Si/Ge ratio of the as-made material becomes closer to that of the mixture. For a Si/(Ge+Al) = 50, the germanium uptake increases with decreasing Ge/Al ratio. For the lowest Si/(Ge+Al) value there is even closer correlation between the Si/Ge ratio of the final materials and the initial mixtures. These results imply that the presence of aluminum increases the uptake of germanium into the zeolite framework. Alternatively, it can be viewed that the germanium, by enhancing the growth kinetics (see below) allows one to increase the aluminum content in the zeolite, resulting in materials with a higher aluminum content that are still crystalline.

Growth Rate of Ge,Al-silicalite-1. SAXS was used to quantify the opposing effects of germanium (enhancing) and aluminum (suppressing) on silicalite-1 growth rates. The time-resolved scattering patterns and the particle sizes versus time for Si/(Ge+Al) = 100 are shown in Figures 9 and 10 (the remainder of the data is in the Supporting Information). The main parameters are summarized in Table 4. At low heteroatom content (Si/(Ge+Al) = 100), the induction period and the time elapsed until Bragg peaks are first observed in the Porod regime are approximately 6.0 and 13.5 h, respectively, yielding a growth rate of 2.39 ± 0.06 nm/h at Ge/Al = 4. No difference in the growth rate could be observed when the aluminum content is increased at the same total heteroatom content. More specifically for Si/(Ge+Al) = 100 and Ge/Al = 1 the induction period and the time elapsed until Bragg peaks are first observed in the Porod regime are 7.5 and 15.0 h, giving a growth rate of 2.33 ± 0.07 nm/h. The Ge/Al ratio has only a minor effect in the range studied here, and both of these growth rates are larger than that of the pure silica material. Thus, under these conditions the growth behavior appears to be in line with what would be expected from the single-substituted materials. Germanium enhances growth, and at this low level of substitution, aluminum has only a minor effect.

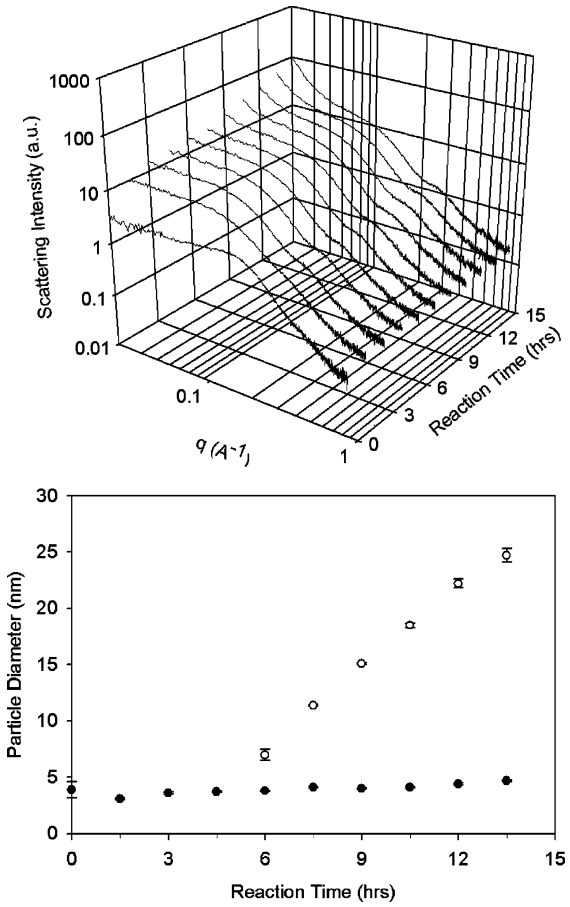

Figure 9. (Top) Time-resolved SAXS scattering patterns of 0.9901 TEOS: 0.0079 GeO_2: 0.0020 $Al(OC_2H_5)_3$: 0.36 TPAOH: 20 H_2O at 368 K. (Bottom) Plot of particle size versus reaction time. Si/(Ge+Al) = 100, Ge/Al = 4.

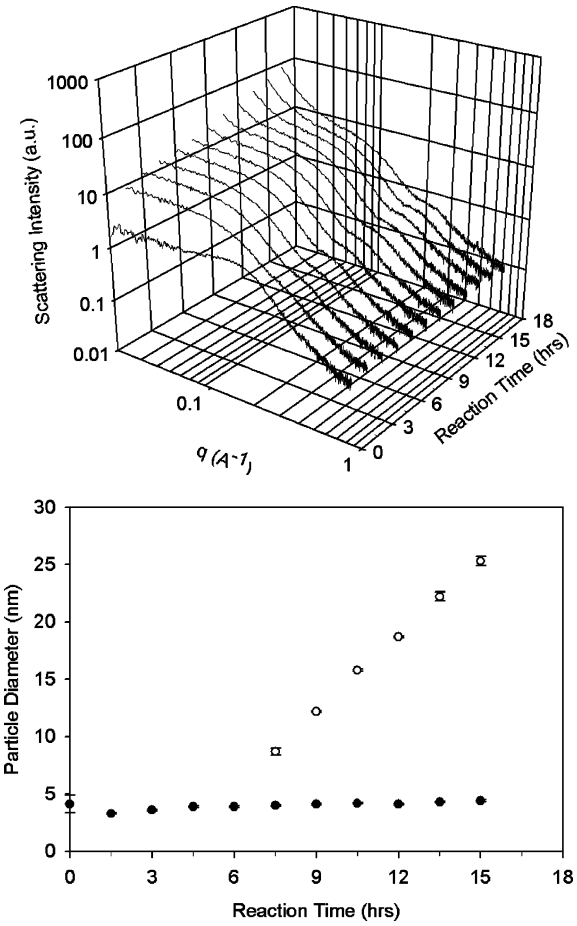

Figure 10. (Top) Time-resolved SAXS scattering patterns of 0.9901 TEOS: 0.0050 GeO_2: 0.0050 $Al(OC_2H_5)_3$: 0.36 TPAOH: 20 H_2O at 368 K. (Bottom) Plot of particle size versus reaction time. Si/(Ge+Al) = 100, Ge/Al = 1.

At a Si/(Ge+Al) ratio of 50, the induction period and the time elapsed until Bragg peaks are first observed in the Porod regime are approximately 7.5 and 15.0 h, respectively, leading to a growth rate of 2.25 ± 0.06 nm/h at high germanium content (Ge/Al = 4). Increasing the aluminum content (Ge/Al = 2) increases the induction period and the time elapsed until Bragg peaks are first observed in the Porod regime to 9.0 h and 16.5 h, respectively. The particle growth rate decreases to 1.95 ± 0.05 nm/h. Again, the behavior observed for single-substituted materials holds in the case of mixed substitution. At the highest heteroatom content Si/(Ge+Al) = 25 the effect of the aluminum becomes more significant, even at the highest germanium content (Ge/Al = 4). The induction period and time elapsed until Bragg peaks are first observed in the Porod regime are 13.5 and 19.5 h. The particle growth rate is further decreased to 1.78 ± 0.04 nm/h.

To compare these data to the results for pure aluminum incorporation, Table 5 lists the initial scattered intensity at zero angle ($I(0)$) and the ratio of primary particles to growing crystals. Two points stand out. First, the $I(0)$ values (1.7−3.0) are smaller than for the pure silica case but increase with increasing germanium content, indicating, at least qualitatively, a decrease in the number density of primary particles. Second, and more notable, is the large increase in the ratio of primary particles to growing crystals upon reduction of germanium at a fixed total heteroatom content. Again, given the assumptions made, the difference in the numbers is only qualitative, but there is clearly a large difference in the relative amount of growing crystals as the germanium content is varied. This is consistent with the growth rates observed that indicate growth is suppressed at a given heteroatom content as the germanium content is decreased.

TABLE 4: Growth Kinetics Summary of Ge,Al-silicalite-1 from in Situ SAXS Measurements

Si/(Ge+Al) ratio	Ge/Al ratio	duration of induction period (h)	appearance of Bragg diffraction peaks (h)	growth rate (nm/h)
100	4	4.5−6.0	13.5	2.39 ± 0.06
	1	6.0−7.5	15.0	2.33 ± 0.07
50	4	6.0−7.5	15.0	2.25 ± 0.06
	2	7.5−9.0	16.5	1.95 ± 0.05
25	4	12.0−13.5	19.5	1.78 ± 0.04

TABLE 5: Initial Scattered Intensity ($I(0)$) and Estimate of the Ratio of Primary Particles to Growing Crystals of Al-silicalite-1 from in Situ SAXS Measurements

Si/(Ge+Al) ratio	Ge/Al ratio	$I(0)$ before heating	primary particles/ growing crystals[a] ratio
100	4	2.6	2.2 (13.5)
	1	2.1	17.9 (15.0)
50	4	3.0	1.8 (15.0)
	2	1.7	32.7 (16.5)
25	4	2.6	3.8 (19.5)

[a] Heating duration at 368 K (in hours) given in parentheses. In all cases the growing crystals are approximately 25 nm in diameter.

Discussion

The PXRD, XRF, N_2 adsorption, FTIR, and SAXS of the syntheses containing aluminum show that the presence of

aluminum in the synthesis mixture has a deleterious effect on zeolite formation, both in the rate of formation and the crystallinity of the material obtained. It is interesting to note that the Si/Al ratio of the final product is comparable to that of the original mixture; this is not true in the case of solutions containing germanium. It is also interesting to note that the trend of decreasing crystallinity at increasing heteroatom content is also observed for many high silica zeolites made under conventional conditions (high temperatures, presence of alkali, lower pH values),[5] although *not* for ZSM-5. As such, the clear solution syntheses of Al-silicalite-1 behave as "conventional" mixtures in regards to aluminum content and crystallinity. Two possible reasons for the decrease in crystallinity with increasing aluminum content is the absence of alkali cations such as sodium or the high pH of the synthesis mixtures.

The results for the mixed substitution materials have implications for Ge,Al-MFI zeolites used as catalysts. Under the conditions studied here the presence of aluminum facilitates the incorporation of germanium. The pH of the germanium- and aluminum-containing mixtures should not be dramatically different than those without aluminum, but that in essence seems to be the effect (germanium solubility decreases with decreasing pH). Also the growth rates of the ternary (Ge,Al,Si) zeolites can be clearly understood on the basis of the results of the Ge,-Si and Al,Si zeolites: germanium enhances growth, aluminum suppresses growth. Given that nearly all previous studies of Ge,-Al-mixed substitution in silicalite-1 were performed using fluoride-mediated syntheses, most notably work from Maschmeyer's lab,[22] the results of this work are compared with a similar system investigated by Ovejero's group, in which simultaneous incorporation of aluminum and titanium into MFI was studied.[43] Interestingly, in that case titanium incorporation depended on the Si/Al and Si/Ti ratios of the initial composition. In contrast to the current work, the presence of aluminum hindered the incorporation of Ti atoms in the MFI framework.

It is also worthwhile to comment on the current results in the context of numerous recent works on dilute, clear solution syntheses of silicalite-1.[10,12,19,21,41,44,45] In agreement with those works as well as many studies of concentrated clear solutions,[16−18,46] there are small (<5 nm) particles present from the initial stages of synthesis. Upon heating a second population of particles, it is observed that they continue to grow throughout the heating period. This work clearly shows that the presence of aluminum has a deleterious effect on zeolite growth and that, to a first approximation, the germanium and aluminum in the ternary system effects on growth can be reasonably predicted from their behavior in binary mixtures. The notable exception to this is germanium uptake increases at the higher heteroatom content in the presence of aluminum as compared to mixtures containing just germanium.[8] One result, in contrast to the work by Davis and co-workers, is that the ratio of primary to growing particles is on the order of one for the case of high Ge/Al ratios (4). In their report, the growing crystals were a very small percentage, typically less than 5%, of the total number of particles. Interestingly in the Ge,Al mixtures with low germanium content (Ge/Al = 1), the ratio of primary to growing particles is more in line with what is observed in their work. This result indicates the relative number of growing particles is strongly affected by the Ge/Al ratio. Whether the larger particles observed in this work form by aggregation of the small primary particles, as shown in previous work for dilute silicalite-1 mixtures,[19,21] is unknown.

Conclusions

The incorporation of aluminum and the simultaneous incorporation of germanium and aluminum in the MFI framework can be achieved using clear solution syntheses. The incorporation rate of aluminum is independent of the initial Si/Al ratio under the conditions investigated here. The incorporation rate of germanium is enhanced in the presence of aluminum, especially with increasing heteroatom content. Aluminum in the synthesis mixture decreases the growth rate of silicalite-1 in contrast to germanium which enhances the growth rate. The influence of the heteroatoms in syntheses with mixed substitution can be understood on the basis of the single-substituted mixtures, with the notable exception of the enhanced germanium uptake into the zeolite. The results above provide fundamental insights about how one can design silicalite-1 nanoparticles with sufficient heteroatom content to be relevant for catalysis. Ongoing work is exploring this avenue and will be reported elsewhere.

Acknowledgment. We acknowledge financial support from Texas A&M University and SABIC USA Inc. The SAXS instruments were purchased from funds obtained under NSF Grant CTS-0215838. We acknowledge the X-ray Diffraction Facility at Texas A&M University for access to the XRD and SAXS instruments and Seunguk Yeu for acquiring the FE-SEM images. The FE-SEM instrument was supported by the National Science Foundation under Grant DBI-0116835.

Supporting Information Available: Calculation of the ratio of primary particles to growing crystals from the SAXS data, table of XRF results, adsorption data summary, FE-SEM of Ge,-Al-silicalite-1 samples, FTIR spectra of all samples, time-resolved SAXS scattering patterns for Ge,Al-silicalite-1 (Si/(Al+Ge) = 50, in which Ge/Al = 4 and 2, and Si/(Al+Ge) = 25, in which Ge/Al = 4) and the corresponding plots of particle size versus reaction time. This material is available free of charge via the Internet at http://pubs.acs.org.

References and Notes

(1) Barrer, R. M. *Hydrothermal Chemistry of Zeolites*; Academic Press: London, 1982.
(2) Breck, D. W. *Zeolite Molecular Sieves: Structure, Chemistry and Use*; Wiley: New York, 1974.
(3) Wagner, P.; Nakagawa, Y.; Lee, G. S.; Davis, M. E.; Elomari, S.; Medrud, R. C.; Zones, S. I. *J. Am. Chem. Soc.* **2000**, *122*, 263−273.
(4) Zones, S. I.; Hwang, S. J.; Davis, M. E. *Chem.−Eur. J.* **2001**, *7*, 1990−2001.
(5) Zones, S. I.; Nakagawa, Y.; Lee, G. S.; Chen, C. Y.; Yuen, L. T. *Microporous Mesoporous Mater.* **1998**, *21*, 199−211.
(6) Zones, S. I.; Nakagawa, Y.; Yuen, L. T.; Harris, T. V. *J. Am. Chem. Soc.* **1996**, *118*, 7558−7567.
(7) Nakagawa, Y.; Lee, G. S.; Harris, T. V.; Yuen, L. T.; Zones, S. I. *Microporous Mesoporous Mater.* **1998**, *22*, 69−85.
(8) Cheng, C.-H.; Juttu, G.; Mitchell, S.; Shantz, D. F. *J. Phys. Chem. B* **2006**, *110*. In press..
(9) Mintova, S.; Valtchev, V. *Microporous Mesoporous Mater.* **2002**, *55*, 171−179.
(10) Nikolakis, V.; Tsapatsis, M.; Vlachos, D. G. *Langmuir* **2003**, *19*, 4619−4626.
(11) Persson, A. E.; Schoeman, B. J.; Sterte, J.; Ottesstedt, J. E. *Zeolites* **1994**, *14*, 557−567.
(12) Rimer, J. D.; Vlachos, D. G.; Lobo, R. F. *J. Phys. Chem. B* **2005**, *109*, 12762−12771.
(13) Schoeman, B. J. *Microporous Mesoporous Mater.* **1997**, *9*, 267−271.
(14) Schoeman, B. J. *Zeolites* **1997**, *18*, 97−105.
(15) Schoeman, B. J. *Stud. Surf. Sci. Catal.* **1997**, *105*, 647−654.
(16) Schoeman, B. J. *Microporous Mesoporous Mater.* **1998**, *22*, 9−22.
(17) Schoeman, B. J.; Regev, O. *Zeolites* **1996**, *17*, 447−456.
(18) Schoeman, B. J.; Sterte, J.; Otterstedt, J. E. *Zeolites* **1994**, *14*, 568−575.

(19) Davis, T. M.; Drews, T. O.; Ramanan, H.; He, C.; Dong, J.; Schnablegger, H.; Katsoulakis, M. A.; Kokkoli, E.; McCormick, A. V.; Lee Penn, R.; Tsapatsis, M. *Nat. Mater.* **2006**, *5*, 400−408.

(20) Hsu, C. Y.; Chiang, A. S. T.; Selvin, R.; Thompson, R. W. *J. Phys. Chem. B* **2005**, *109*, 18804−18814.

(21) Nikolakis, V.; Kokkoli, E.; Tirrell, M.; Tsapatsis, M.; Vlachos, D. G. *Chem. Mater.* **2000**, *12*, 845−853.

(22) van de Water, L. G. A.; van der Waal, J. C.; Jansen, J. C.; Cadoni, M.; Marchese, L.; Maschmeyer, T. *J. Phys. Chem. B* **2003**, *107*, 10423−10430.

(23) van de Water, L. G. A.; van der Waal, J. C.; Jansen, J. C.; Maschmeyer, T. *J. Catal.* **2004**, *223*, 170−178.

(24) van de Water, L. G. A.; Zwijnenburg, M. A.; Sloof, W. G.; van der Waal, J. C.; Jansen, J. C.; Maschmeyer, T. *ChemPhysChem* **2004**, *5*, 1328−1335.

(25) Gregg, S. J.; Sing, K. S. W. *Adsorption, Surface Area and Porosity*; Academic Press: London, 1982.

(26) Rouquerol, F.; Rouquerol, J.; Sing, K. *Adsorption by Powders and Porous Solids*; Academic Press: London, 1999.

(27) Cheng, C.-H.; Shantz, D. F. *J. Phys. Chem. B* **2005**, *109*, 13912−13920.

(28) Cheng, C.-H.; Shantz, D. F. *J. Phys. Chem. B* **2005**, *109*, 19116−19125.

(29) Glatter, O. *J. Appl. Crystallogr.* **1977**, *10*, 415−421.

(30) Glatter, O. *J. Appl. Crystallogr.* **1979**, *12*, 166−173.

(31) Glatter, O. *J. Appl. Crystallogr.* **1980**, *13*, 7−11.

(32) Glatter, O. *J. Appl. Crystallogr.* **1980**, *13*, 577−584.

(33) Glatter, O.; Kratky, O. *Small Angle X-ray Scattering*; Academic Press: London, 1982.

(34) Svergun, D. I. *J. Appl. Crystallogr.* **1992**, *25*, 495−503.

(35) Guinier, A.; Fournet, G. *Small-Angle Scattering of X-rays*; John Wiley & Sons: New York, 1955.

(36) Kragten, D. D.; Fedeyko, J. M.; Sawant, K. R.; Rimer, J. D.; Vlachos, D. G.; Lobo, R. F.; Tsapatsis, M. *J. Phys. Chem. B* **2003**, *107*, 10006−10016.

(37) Schlenker, J. L.; Peterson, B. K. *J. Appl. Crystallogr.* **1996**, *29*, 178−185.

(38) Watson, J. N.; Iton, L. E.; Keir, R. I.; Thomas, J. C.; Dowling, T. L.; White, J. W. *J. Phys. Chem. B* **1997**, *101*, 10094−10104.

(39) Cheng, C.-H.; Shantz, D. F. *J. Phys. Chem. B* **2005**, *109*, 19116−19125.

(40) Cundy, C. S.; Lowe, B. M.; Sinclair, D. M. *Faraday Discuss.* **1993**, *95*, 235−252.

(41) Fedeyko, J. M.; Rimer, J. D.; Lobo, R. F.; Vlachos, D. G. *J. Phys. Chem. B* **2004**, *108*, 12271−12275.

(42) Iler, R. K. *The Chemistry of Silica*; John Wiley & Sons: New York, 1979.

(43) Ovejero, G.; van Grieken, R.; Uguina, M. A.; Serrano, D. P.; Melero, J. A. *J. Mater. Chem.* **1998**, *8*, 2269−2276.

(44) Rimer, J. D.; Lobo, R. F.; Vlachos, D. G. *Langmuir* **2005**, *21*, 8960−8971.

(45) Fedeyko, J. M.; Vlachos, D. G.; Lobo, R. F. *Langmuir* **2005**, *21*, 5197−5206.

(46) Yang, S.; Navrotsky, A.; Wesolowski, D.; Pople, J. A. *Chem. Mater.* **2004**, *16*, 210−219.